Imaging of the cross-presenting dendritic cell subsets in the skin-draining lymph node

Masahiro Kitano[a,b], Chihiro Yamazaki[c,d,e], Akiko Takumi[a], Takashi Ikeno[a,f], Hiroaki Hemmi[c,g,h,i], Noriko Takahashi[a], Kanako Shimizu[j], Scott E. Fraser[b], Katsuaki Hoshino[c,g,h,k], Tsuneyasu Kaisho[c,d,g,h,i,1], and Takaharu Okada[a,l,m,1]

[a]Laboratory for Tissue Dynamics, RIKEN Center for Integrative Medical Sciences, Yokohama, Kanagawa 230-0045, Japan; [b]Translational Imaging Center, University of Southern California, Los Angeles, CA 90089; [c]Laboratory for Host Defense, RIKEN Research Center for Allergy and Immunology, Yokohama, Kanagawa 230-0045, Japan; [d]Department of Allergy and Immunology, Graduate School of Medicine, Osaka University, Suita, Osaka 565-0871, Japan; [e]Department of Immunology, Graduate School of Medicine, Dentistry, and Pharmaceutical Sciences, Okayama University, Okayama, Okayama 700-8558, Japan; [f]Laboratory of Lymphocyte Differentiation, Graduate School of Frontier Biosciences, Osaka University, Suita, Osaka 565-0871, Japan; [g]Laboratory for Inflammatory Regulation, RIKEN Center for Integrative Medical Sciences, Yokohama, Kanagawa 230-0045, Japan; [h]Laboratory for Immune Regulation, World Premier International Research Center Initiative, Immunology Frontier Research Center, Osaka University, Suita, Osaka 565-0871, Japan; [i]Department of Immunology, Institute of Advanced Medicine, Wakayama Medical University, Wakayama, Wakayama 641-8509, Japan; [j]Laboratory for Immunotherapy, RIKEN Center for Integrative Medical Sciences, Yokohama, Kanagawa 230-0045, Japan; [k]Department of Immunology, Faculty of Medicine, Kagawa University, Miki, Kagawa 761-0793, Japan; [l]Precursory Research for Embryonic Science and Technology, Japan Science and Technology Agency, Saitama, Saitama 332-0012, Japan; and [m]Graduate School of Medical Life Science, Yokohama City University, Yokohama 230-0045, Japan

Edited by Ira Mellman, Genentech, Inc., South San Francisco, CA, and approved November 30, 2015 (received for review July 11, 2015)

Dendritic cells (DCs) are antigen-presenting cells specialized for activating T cells to elicit effector T-cell functions. Cross-presenting DCs are a DC subset capable of presenting antigens to $CD8^+$ T cells and play critical roles in cytotoxic T-cell–mediated immune responses to microorganisms and cancer. Although their importance is known, the spatiotemporal dynamics of cross-presenting DCs in vivo are incompletely understood. Here, we study the T-cell zone in skin-draining lymph nodes (SDLNs) and find it is compartmentalized into regions for $CD8^+$ T-cell activation by cross-presenting DCs that express the chemokine (C motif) receptor 1 gene, *Xcr1* and for $CD4^+$ T-cell activation by $CD11b^+$ DCs. *Xcr1*-expressing DCs in the SDLNs are composed of two different populations: migratory ($CD103^{hi}$) DCs, which immigrate from the skin, and resident ($CD8\alpha^{hi}$) DCs, which develop in the nodes. To characterize the dynamic interactions of these distinct DC populations with $CD8^+$ T cells during their activation in vivo, we developed a photoconvertible reporter mouse strain, which permits us to distinctively visualize the migratory and resident subsets of *Xcr1*-expressing DCs. After leaving the skin, migratory DCs infiltrated to the deep T-cell zone of the SDLNs over 3 d, which corresponded to their half-life in the SDLNs. Intravital two-photon imaging showed that after soluble antigen immunization, the newly arriving migratory DCs more efficiently form sustained conjugates with antigen-specific $CD8^+$ T cells than other *Xcr1*-expressing DCs in the SDLNs. These results offer in vivo evidence for differential contributions of migratory and resident cross-presenting DCs to $CD8^+$ T-cell activation.

dendritic cell | $CD8^+$ T cell | cross-presentation | intravital two-photon imaging | photoconversion

Dendritic cells (DCs) play critical roles in shaping T-cell responses as they present antigenic peptides and provide the requisite costimulatory signals for T-cell activation (1). In primary immune responses, naive T cells receive these antigen and costimulatory signals by physically interacting with DCs in secondary lymphoid tissues such as lymph nodes (LNs). Recent advances in intravital imaging techniques using two-photon excitation fluorescent microscopy reveal the dynamic DC and T-cell behaviors during T-cell activation. When naive T cells encounter DCs presenting sufficient amounts of antigenic peptides, they reduce their motility and attach to the DCs for prolonged periods of time, ranging from 10 min to hours (2–4). A limitation of previous imaging studies was the inability to visually distinguish endogenous DC subpopulations that are distinct from one another in phenotype and function (5–7). This has clouded the ability of the studies to define the relative contributions of the different DC subsets in T-cell activation.

Cytotoxic T cells, which play critical roles in the defense against microorganisms and cancer, are generated from $CD8^+$ T cells through interactions with relatively small populations of DCs. In LNs, it is the $CD8\alpha^+CD103^+$ class of DCs that is capable of cross-presenting exogenous antigen-derived peptides on major histocompatibility complex (MHC) class I, making them important for $CD8^+$ T-cell responses. Other DC subsets, including $CD11b^+$ DCs, are mainly involved in $CD4^+$ T-cell responses (5, 8, 9). Among $CD8\alpha^+CD103^+$ DCs, $CD8\alpha^{hi}CD103^{int}$ DCs are a LN-resident population (hereafter called LN-resident DCs or $CD8\alpha^{hi}$ DCs) whereas $CD8\alpha^{int}CD103^{hi}$ DCs are a migratory subset derived from peripheral tissues (hereafter called migratory DCs or $CD103^{hi}$ DCs). The migratory DCs constantly immigrate from the skin to the skin-draining LNs (SDLNs). Upon activation by innate stimuli, e.g., double-stranded RNAs, the skin migratory DCs increase their rate of immigration to the SDLNs (10). The first compelling evidence for the differential distribution of distinct DC populations in LNs was reported a decade ago (11). Until recently, however, the distribution of $CD8\alpha^{hi}$ DCs and $CD103^{hi}$ DCs could not be studied because of the difficulty in histologically identifying these cells in LNs. Computational processing of

Significance

This work, for the first time to our knowledge, distinctly visualizes the two different populations of dendritic cells (DCs) essential for cytotoxic T-cell generation in the skin-draining lymph nodes (SDLNs): the migratory $CD103^{hi}$ DCs that immigrate from other organs including the skin and the $CD8\alpha^{hi}$ DCs that are resident in the SDLNs. By imaging the spatiotemporal dynamics of the migratory and resident subsets of DCs in the SDLNs, we find that these two different populations play different roles in antigen presentation, with the migratory DCs being dramatically more potent in interacting with $CD8^+$ T cells. This work offers critical insights into several areas, including optimizing vaccines for microbes and tumors.

Author contributions: M.K., T.K., and T.O. designed research; M.K., A.T., T.I., N.T., and T.O. performed research; C.Y., H.H., K.S., K.H., and T.K. contributed new reagents/analytic tools; M.K. and T.O. analyzed data; and M.K., S.E.F., T.K., and T.O. wrote the paper.

The authors declare no conflict of interest.

This article is a PNAS Direct Submission.

Freely available online through the PNAS open access option.

[1]To whom correspondence may be addressed. Email: takaharu.okada@riken.jp or tkaisho@wakayama-med.ac.jp.

This article contains supporting information online at www.pnas.org/lookup/suppl/doi:10.1073/pnas.1513607113/-/DCSupplemental.

multicolor histological images suggested that these cross-presenting DC subsets were preferentially accumulated in deep areas of the T-cell zone in the SDLNs (12). Other studies directly visualized both DC subsets by histological analyses of chemokine (C motif) receptor 1 (XCR1) expression, which is selectively and highly expressed in both LN-resident DCs and migratory DCs (13–16). These studies have demonstrated the differential localization of cross-presenting DCs and other types of DCs in the SDLNs.

Despite the above advances, there remain many open questions concerning the interactions of DCs and T cells. For example, it is not known whether the activation of $CD8^+$ T cells and $CD4^+$ T cells in the SDLNs is spatially coordinated according to the differential localization of cross-presenting DCs and other DCs. Moreover, little is known about the dynamics of migratory DCs in the SDLNs. In addition, it is difficult to compare the contributions of LN-resident DCs and migratory DCs to $CD8^+$ T-cell activation in the SDLNs. Only somewhat indirect assays have been used; for example, an ex vivo assay using DCs sorted from the SDLNs has been used to study the events of herpes simplex virus type 1 (HSV-1) infection (17). For soluble protein vaccination, the DC subsets that most contribute to $CD8^+$ T-cell activation in the SDLNs remain unknown. Soluble protein antigens administered s.c. are delivered to the SDLNs not only by skin DCs but also via lymph flow in lymphatic sinuses and LN conduits, permitting DCs in the SDLNs to sample them (18, 19). Mechanical disruption of LNs for the ex vivo assay may artificially expose irrelevant DC subsets to soluble protein antigens. Thus, it is important to establish the in vivo assay system to evaluate the differential roles for the migratory and LN-resident DC subsets in $CD8^+$ T-cell activation.

In this study, we have used direct imaging approaches to determine the locations for activation of $CD8^+$ T cells and $CD4^+$ T cells in the SDLNs. Using newly generated reporter mice expressing a photochromic fluorescent protein in DCs that express the XCR1 gene (*Xcr1*), we have developed a method to distinctively visualize the LN-resident DCs and migratory DCs in the SDLNs. Intravital microscopy has been used to analyze cognate interactions of the DC subsets with $CD8^+$ T cells after immunization with soluble antigen. Our results provide insights into the DC inter- and intratissue migration dynamics, which are associated with in vivo contributions of different DC subsets to $CD8^+$ T-cell activation.

Results

Regionalization of *Xcr1*-Expressing DCs in the SDLNs. We histologically analyzed the localization of cross-presenting DCs in the SDLNs by using $Xcr1^{Venus/+}$ mice, in which the coding region of the *Xcr1* gene was replaced with a gene encoding the yellow fluorescent protein Venus (16). *Xcr1*-expressing DCs were found enriched in deep parts of the T-cell zone (Fig. 1*A*). *Xcr1*-expressing DCs were sparse in regions of the T-cell zone proximal to B-cell follicles or medullary regions, where many high endothelial venules (HEVs) and $CD11b^+$ DCs were enriched (Fig. 1 *A* and *B* and Fig. S1*A*). These results are consistent with the previous multicolor histological analyses of cross-presenting DCs (12). $Xcr1^{Venus/Venus}$ cross-presenting DCs were found localized normally in the deep parts of the T-cell zone, indicating that XCR1 expression was not required for the localization (Fig. S1*B*).

To investigate the relationship between the differential localization of the DC subsets and activation of $CD8^+$ T cells and $CD4^+$ T cells, we cotransferred ovalbumin (OVA)-specific TCR transgenic $CD8^+$ (OT-I) T cells (20) and OVA-specific TCR transgenic $CD4^+$ (OT-II) T cells (21) to $Xcr1^{Venus/+}$ mice. Before immunization, OT-I T cells and OT-II T cells seemed to be evenly distributed throughout the T-cell zone (Fig. 1*C*). However, quantitative analysis to measure the distance between individual antigen-specific T cells and the centroid of the Xcr1-expressing DC area showed that OT-I T cells were distributed slightly but significantly closer to the Xcr1-expressing DC area centroid than

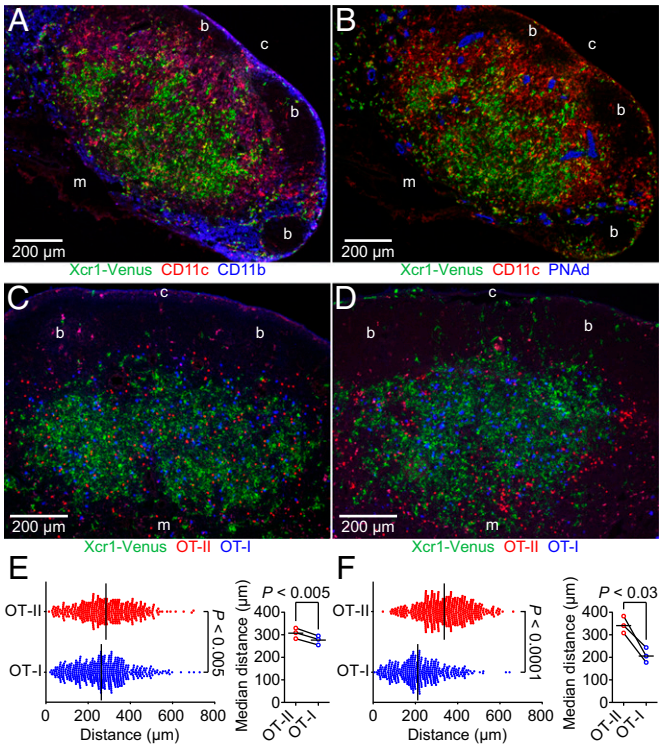

Fig. 1. Localization of *Xcr1*-expressing DCs and spatial segregation of antigen-engaged $CD8^+$ T cells and $CD4^+$ T cells in the SDLNs. (*A* and *B*) Immunofluorescence images of serial inguinal LN sections from an unimmunized $Xcr1^{Venus/+}$ mouse. Fig. S1 shows the grayscale images of the individual fluorescence channels in *A*. (*C* and *D*) Fluorescence images of inguinal LN sections from $Xcr1^{Venus/+}$ mice transferred with 5×10^6 DiD-labeled OT-I T cells and 5×10^6 tdTomato$^+$ OT-II T cells. The LN sections are from an unimmunized mouse (*C*) and a mouse s.c. immunized with soluble OVA plus poly(I:C) for 24 h (*D*). "b," "c," and "m" indicate B-cell follicle, cortical side, and medullary side, respectively. (*E* and *F*) (*Left*) Distances between the *Xcr1*-Venus$^+$ cell area centroid and individual OT-I or OT-II T cells. Each symbol represents one cell. Bars indicate median values in each group. Data are pooled from three images of different lymph nodes from unimmunized mice (*E*) or mice immunized with OVA plus poly(I:C) for 24 h (*F*). Fig. S1 *C* and *D* shows the processed images used for data analysis. Bars indicate mean values in each group.

OT-II T cells (Fig. 1*E* and Fig. S1*C*). Although priming of OT-I T cells seemed to be slower than that of OT-II T cells after immunization with soluble OVA plus double-stranded RNA analog poly (I:C) adjuvant, the majority of both OT-I and OT-II T cells had up-regulated CD69 and CD25 by about 1 d postimmunization (Fig. S1 *E* and *F*). At this time point, OT-I T cells accumulated in the *Xcr1*-expressing DC-rich region whereas OT-II T cells were mostly localized in the *Xcr1*-expressing DC-sparse region (Fig. 1 *D* and *F* and Fig. S1*D*). These results indicate that the T-cell zone is compartmentalized into subregions for cognate interactions of $CD8^+$ T cells with *Xcr1*-expressing DCs and for cognate interactions of $CD4^+$ T cells with $Xcr1^-$ DCs. They also suggest that migration of naive $CD8^+$ T cells and $CD4^+$ T cells in the T-cell zone is biased to facilitate scanning for their cognate DCs.

***Xcr1*-Expressing DCs Are the Main Interaction Partners of Antigen-Specific $CD8^+$ T Cells.** We analyzed the interaction dynamics between *Xcr1*-expressing DCs and antigen-specific $CD8^+$ T cells with intravital two-photon excitation fluorescence microscopy of the SDLNs. $Xcr1^{Venus/+}$ mice were cotransferred with GFP-expressing OT-I T cells and tdTomato-expressing polyclonal $CD8^+$ T cells. One day later, the mice were s.c. immunized with soluble OVA plus poly(I:C). Further entry of lymphocytes into the SDLNs was

blocked by i.v. injection of anti-CD62L antibody at 2 h after the immunization. OT-I T cells exhibited similar motility to polyclonal $CD8^+$ T cells until 8 h postimmunization but started to decrease it by 12 h after immunization. By 18–26 h postimmunization, the majority of OT-I T cells became much more sessile, moving at a median velocity of ≤4 μm/min (Fig. 2 *A* and *B* and Movie S1), which suggests their sustained interactions with cognate antigen-presenting cells. Indeed, more than 90% of the sessile OT-I T cells were seen to form stable contacts with *Xcr1*-Venus$^+$ DCs (Fig. 2*C*, Fig. S2*A*, and Movie S2). Interestingly, some *Xcr1*-Venus$^+$ DCs seemed to be interacting with multiple OT-I T cells, whereas some of the other *Xcr1*-Venus$^+$ DCs were not in stable contacts with OT-I T cells (Fig. 2*A*, Fig. S2*A*, and Movie S2). After 46 h of immunization, OT-I T cells swelled and regained their motility (Fig. 2 *A* and *B* and Movie S1). These results are largely consistent with the previous imaging reports about interactions between antigen-specific $CD8^+$ T cells and peptide-pulsed DCs (3) and suggest that it takes 8–12 h for the emergence in the SDLNs of DCs that have cross-presented significant amounts of OVA.

To confirm that the interaction with *Xcr1*-expressing DCs is important for antigen-specific $CD8^+$ T-cell activation, we used $Xcr1^{DTRVenus/+}$ mice to deplete *Xcr1*-expressing DCs (16) and evaluated its impact on the proliferation of antigen-specific $CD8^+$ T cells upon immunization. Both $Xcr1^{+/+}$ mice and $Xcr1^{DTRVenus/+}$ mice were cotransferred with OT-I T cells and OT-II T cells and treated with diphtheria toxin (DT) on day −1. The mice were s.c. immunized with soluble OVA plus poly(I:C) on day 0, additionally treated with DT on day 1 and day 3, and killed for flow cytometric analysis of the SDLNs on day 4. This resulted in 86 ± 2.2% ($n = 3$) depletion of cross-presenting DCs (total number of LN-resident DCs and migratory DCs) in the SDLNs of $Xcr1^{DTRVenus/+}$ mice. The number of OT-I T cells but not that of OT-II T cells was much reduced in the LNs of $Xcr1^{DTRVenus/+}$ mice compared with $Xcr1^{+/+}$ mice (Fig. S2*B*). These results indicate that *Xcr1*-expressing DCs are the primary interaction partners of antigen-specific $CD8^+$ T cells in the SDLNs upon soluble antigen immunization.

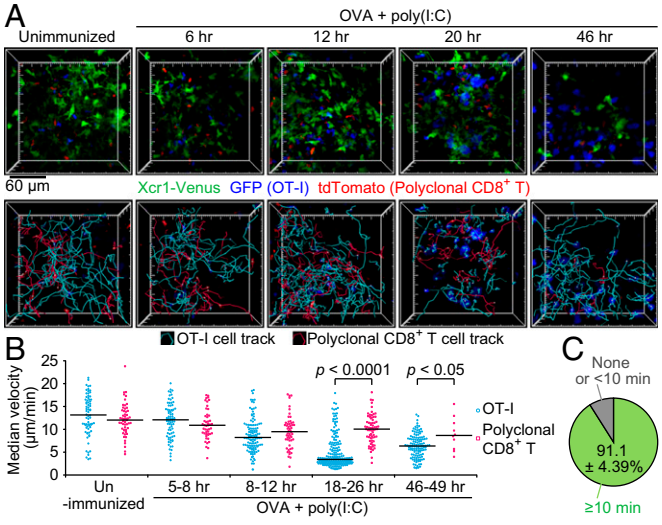

Fig. 2. *Xcr1*-expressing DCs are the main interaction partners of antigen-specific $CD8^+$ T cells. $Xcr1^{Venus/+}$ mice were cotransferred with 4×10^6 GFP^+ OT-I T cells and 1×10^6 $tdTomato^+$ polyclonal $CD8^+$ T cells, s.c. immunized with soluble OVA plus poly(I:C), and subjected to intravital imaging of inguinal LNs. (*A*) The 3D-rendered fluorescence images, OT-I T-cell tracks, and polyclonal $CD8^+$ T-cell tracks at the indicated time postimmunization. Imaging duration, 30 min; image depth, 75 μm (Movie S1). (*B*) Median velocity of OT-I T cells and polyclonal $CD8^+$ T cells. Each symbol represents one cell. Bars indicate median values in each group. Data are pooled from at least two imaging sessions in different LNs. (*C*) Percentage of OT-I T cells stably interacting with *Xcr1*-expressing DCs in low-motility OT-I T cells (Fig. S2*A* and Movie S2). Values represent mean ± SEM ($n = 3$; 46, 18, and 69 low-motility OT-I T cells scored in each experiment).

Next we tested the function of XCR1 expressed by DCs in $CD8^+$ T-cell responses. We transferred OT-I T cells to $Xcr1^{Venus/+}$ mice and $Xcr1^{Venus/Venus}$ mice. On day 3 and day 15 after immunization with soluble OVA plus poly(I:C), we found no significant reduction in the OT-I T-cell number in draining LNs from $Xcr1^{Venus/Venus}$ mice compared with $Xcr1^{Venus/+}$ mice (Fig. S2*C*). The deficiency of XCL1, a ligand for XCR1, in $CD8^+$ T cells was reported to impair sustainment of antigen-engaged $CD8^+$ T cells by 12 d after immunization (15). The reason for the seemingly contradictory results to those of the previous report is uncertain at this point, but it might be because of the different adjuvant types used for immunization or because of the potential existence of other unknown receptors for XCL1.

Photoconversion-Based Fluorescent Labeling of *Xcr1*-Expressing Resident $CD8\alpha^{hi}$ DCs and Migratory *Xcr1*-Expressing $CD103^{hi}$ DCs in the SDLNs. As shown previously (16), *Xcr1*-expressing DCs in the SDLNs consist of two populations: resident $CD8\alpha^{hi}$ ($MHC\text{-}II^{int}$) DCs and migratory $CD103^{hi}$ ($MHC\text{-}II^{hi}$) DCs, the latter of which are absent in the spleen (Fig. S3*A*). To distinguish these two populations in imaging analyses, we generated the $Xcr1^{KikGR/+}$ mouse strain, in which the *Xcr1* coding region was replaced by a gene-encoding photoconvertible fluorescent protein, Kikume Green-Red (KikGR) (Fig. S3 *B* and *C*) (22). To photoconvert the KikGR protein expressed in the migratory *Xcr1*-expressing DCs in the dermis, the skin of the abdomen, lower back, hip, and thigh of $Xcr1^{KikGR/+}$ mice was exposed to violet-blue light. Before skin illumination, *Xcr1*-expressing DCs in the skin and SDLNs were all green fluorescent ($KikG^+KikR^-$) (Fig. 3*A* and Fig. S3 *D* and *E*). Immediately after illumination, $CD103^{hi}$ DCs in the light-exposed skin became red fluorescent ($KikR^+$) (Fig. S3 *D* and *E*). By 1 d after skin illumination, $KikR^+$ cells became detectable in the SDLNs. As anticipated, most, if not all, of the $KikR^+$ cells in the SDLNs were migratory $CD103^{hi}$ DCs (Fig. 3 *A* and *B*). Meanwhile the $KikG^+KikR^-$ cells are a mixed population of migratory $CD103^{hi}$ DCs, which had reached the SDLNs before the skin illumination, and LN-resident $CD8\alpha^{hi}$ DCs (Fig. 3 *A* and *B*). Repeated daily 3-min illumination on the skin resulted in a gradual replacement of the $KikG^+KikR^-$-labeled, migratory $CD103^{hi}$ DC pool in the SDLNs with the $KikR^+$ cells. The LN-resident $CD8\alpha^{hi}$ DCs (green fluorescent; $KikG^+KikR^-$) remained unchanged (Fig. 3 *A* and *B*). After 6 d of daily skin illumination, a near complete demarcation of migratory $CD103^{hi}$ DCs and LN-resident $CD8\alpha^{hi}$ DCs by red fluorescence and green fluorescence, respectively, was achieved in the SDLNs (Fig. 3 *A* and *B*). Thus, it is suggested that a turnover of skin-derived $CD103^{hi}$ DCs in the SDLNs takes at least 6 d (half-life, about 3 d).

We conducted histological analysis of $KikR^+$ DCs and $KikG^+KikR^-$ DCs in the SDLNs. Because of the technical reasons described in *SI Materials and Methods*, we prepared vibratome slices of unfixed LNs instead of cryosections of fixed LNs. After 9 d of daily illumination, when the photoconversion-based color separation of migratory DCs and LN-resident DCs in the SDLNs had been already achieved (Fig. 3 *A* and *B*), the migratory DCs and LN-resident DCs were both found in the deep T-cell zone. LN-resident DCs, but not migratory DCs, were distributed also in other parts of the LNs, including the region close to the LN capsule (Fig. 3*C*). Two-photon microscopy analysis of intact LNs showed that migratory DCs and LN-resident DCs together form the meshwork, through which naive T cells migrate (Fig. S3*F* and Movies S3 and S4).

We tracked the dynamics of *Xcr1*-expressing $CD103^{hi}$ DCs after their arrival in the SDLNs. One day after skin illumination, $KikR^+$ DCs were found in the cortical half of the *Xcr1*-expressing DC-rich area in the T-cell zone (Fig. 3*D*). Two days after

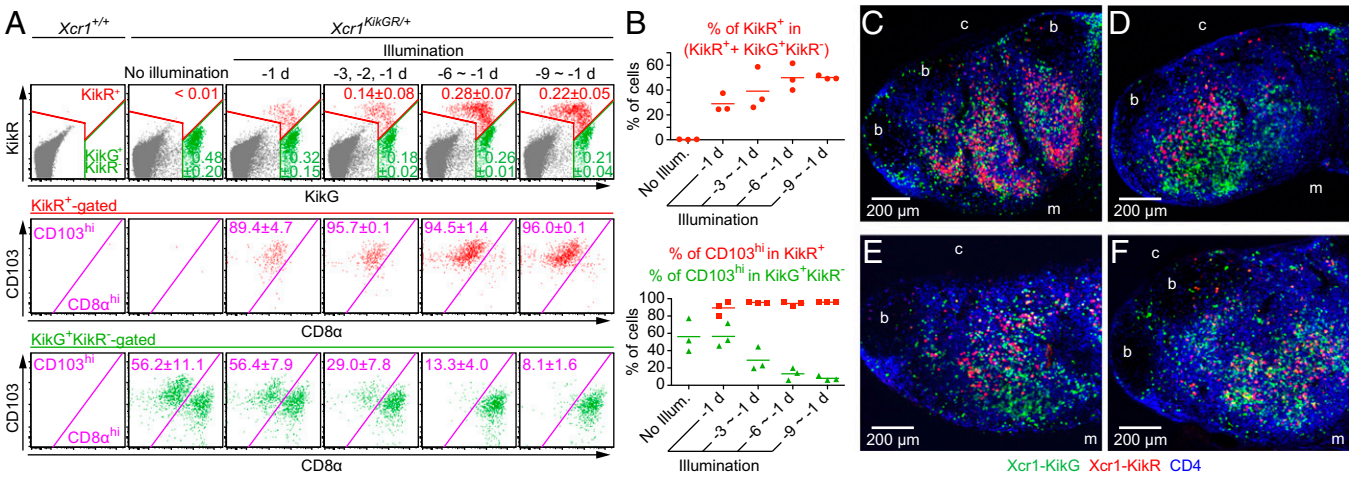

Fig. 3. Photoconversion-based fluorescent labeling of *Xcr1*-expressing CD103^{hi} migratory DCs and *Xcr1*-expressing CD8α^{hi} resident DCs in the SDLNs. (*A*) Flow cytometry of inguinal LN cells from *Xcr1*$^{KikGR/+}$ mice illuminated with violet-blue light at the indicated time points. Values represent mean ± SEM (n = 3). (*B*) Percentage of the indicated cell populations. Each symbol represents one mouse. (*C–F*) Confocal images of halves of inguinal LN sagittal slices from *Xcr1*$^{KikGR/+}$ mice illuminated with violet-blue light once a day for 9 d (*C*), 1 d before analysis (*D*), 2 d before analysis (*E*), and 3 d before analysis (*F*). Shown is an *x–y* plane approximately 20 μm deep from the vibratome slice surface. "b," "c," and "m" indicate B-cell follicle, cortical side, and medullary side, respectively.

illumination, KikR$^+$ DCs infiltrated more extensively in the *Xcr1*-expressing DC-rich area, and 3 d after illumination, some of them reached the most medullary side of the T-cell zone (Fig. 3 *E* and *F*). These results indicate that after leaving the skin, migratory DCs infiltrate into the deep T-cell zone of the SDLNs in 3 d.

Antigen-Specific CD8$^+$ T Cells Preferentially Interact with Migratory CD103^{hi} DCs That Have Newly Arrived in the SDLNs. We sought to determine which *Xcr1*-expresssing DC subset is most efficiently engaged in interactions with antigen-specific CD8$^+$ T cells after immunization. The migratory DCs in the SDLNs can be further subdivided into subpopulations: the migratory DCs newly arriving in the LNs after the immunization and the migratory DCs that have already reached the LNs before immunization. To visualize the distributions of antigen-specific CD8$^+$ T cells and the migratory DC subpopulation newly arriving in the SDLNs upon immunization, *Xcr1*$^{KikGR/+}$ mice were transferred with DiD-labeled OT-I T cells. The mice were subsequently illuminated with violet-blue light to photoconvert the migratory DCs in the skin and were immunized s.c. with soluble OVA plus poly(I:C). After 2 h, the mice were i.v. injected with anti-CD62L antibody (Fig. 4*A*). About 1 d after the skin illumination and immunization, KikR$^+$ DCs were again found in the cortical half of the *Xcr1*-expressing DC-rich area. Interestingly, the majority of OT-I T cells were colocalized with the KikR$^+$ DCs (Fig. 4 *B–D*). Flow cytometric analysis has shown that poly(I:C) injection at the time of skin illumination significantly increased the number of KikR$^+$ DCs arriving in the SDLN in 1 d; whereas the number of migratory DCs that had reached the SDLNs before the skin illumination (KikG$^+$KikR$^-$ CD103^{hi} DCs) or that of the LN-resident DCs (KikG$^+$KikR$^-$ CD8α^{hi} DCs) was not significantly changed by poly (I:C) injection (Fig. S4*A*).

To gain molecular insights into the T-cell–DC interactions, we analyzed the surface expression of costimulatory molecules in each DC subset. Without Poly(I:C) injection, expression of the costimulatory molecules CD86 and CD80 was only slightly higher on the migratory DCs newly arriving in the SDLNs (KikR$^+$ DCs) than on the migratory DCs that have reached the nodes before immunization (KikG$^+$KikR$^-$ CD103^{hi} DCs) and LN-resident DCs (KikG$^+$KikR$^-$ CD8α^{hi} DCs) (Fig. S4 *B–D*), which suggests that illumination-induced activation of the migratory DCs in the skin was minimal, if any. The slight activation of CD103^{hi} DCs seemed to be caused by the hair removal procedure using depilatory cream rather than by light illumination (Fig. S4 *E* and *F*). One day after Poly(I:C) injection, CD86 and CD80 were up-regulated in all of the three DC subsets, and the up-regulation was most prominent in the migratory DCs newly arriving in the SDLNs (KikR$^+$ DCs) (Fig. S4 *B–D*).

For the direct assessments of stable interactions, we performed intravital imaging of the KikR$^+$ DC-infiltrated region, using the protocol shown in Fig. 4*A*. Among OT-I T cells that had slowed down their migration (median speed less than 4 μm/min, Fig. 2*B*), we found OT-I T cells interacting with (*i*) KikG$^+$KikR$^-$ DCs but not with KikR$^+$ DCs, (*ii*) KikR$^+$ DCs but not with KikG$^+$KikR$^-$ DCs, and (*iii*) both KikG$^+$KikR$^-$ DCs and KikR$^+$ DCs. The number of those in contact with (*ii*) KikR$^+$ DCs but not with KikG$^+$KikR$^-$ DCs for more than 10 min was significantly (P < 0.002) more than the number of those in contact with (*i*) KikG$^+$KikR$^-$ DCs but not with KikR$^+$ DCs (Fig. 5 *A–D* and Movies S5 and S6). Because there seemed to be more KikR$^+$ DCs than KikG$^+$KikR$^-$ DCs in the imaging volumes, we normalized the results in Fig. 5*D* by the volumes occupied by KikR$^+$ DCs or

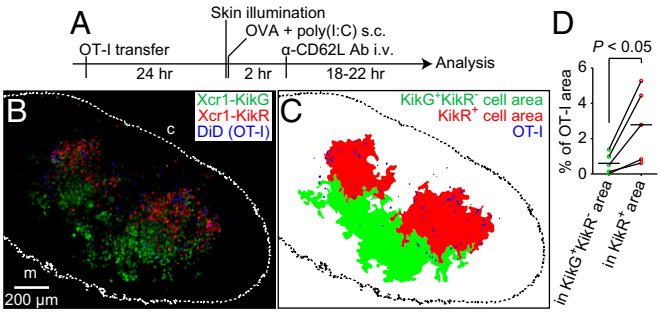

Fig. 4. Antigen-specific CD8$^+$ T cells colocalize with *Xcr1*$^+$ migratory DCs that have arrived in the SDLN after immunization. (*A*) Experimental design. (*B*) A fluorescence image of a half of an inguinal LN sagittal slice from an *Xcr1*$^{KikGR/+}$ mouse treated as described in *A*. A maximal projection image of six confocal sections (35-μm depth) is shown. The dotted line demarcates the LN boundary. "c" and "m" indicate cortical side and medullary side, respectively (*C*) Demarcation of the KikG$^+$KikR$^-$ area, the KikR$^+$ area, and the OT-I T cell–occupied area in the image shown in *B*. See *SI Materials and Methods* for the demarcation method. (*D*) Area occupancy by OT-I T cells in the KikG$^+$KikR$^-$ area and in the KikR$^+$ area calculated from the data in *C* and four other datasets.

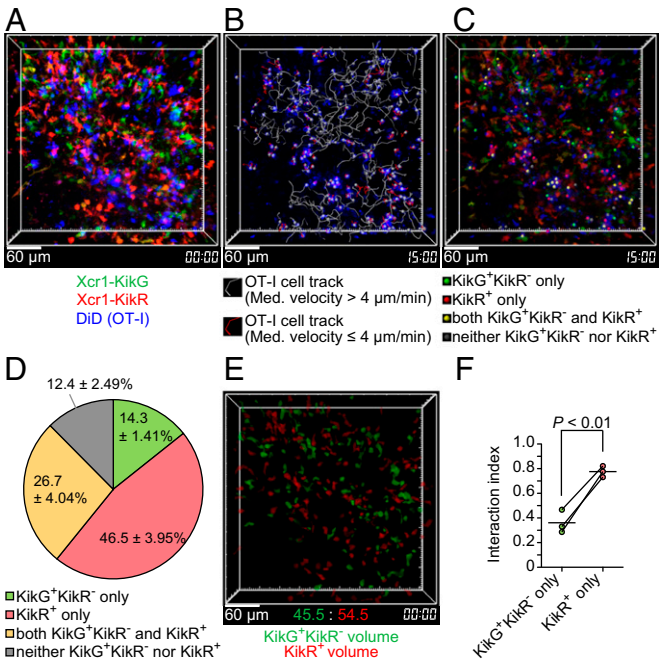

Fig. 5. Antigen-specific CD8$^+$ T cells preferentially interact with *Xcr1*$^+$ migratory DCs that arrived in the SDLN after immunization. (*A*) An intravital two-photon image of an inguinal LN of an *Xcr1*$^{KikGR/+}$ mouse treated as in Fig. 4*A*, except that 8 × 10^6 OT-I T cells were transferred. A 3D-rendered fluorescence image is shown. Image depth: 100 μm (Movie S5). (*B*) OT-I T-cell tracks. Imaging duration: 30 min. (*C*) The interaction partners of low-motility OT-I T cells (median velocity ≤4 μm). The colored dots were placed on low-motility OT-I T cells interacting with the indicated cells (Movie S6). (*D*) Percentage of the interaction partners of low-motility OT-I T cells. Data represent mean ± SEM (n = 3, 43, 113, and 121 stable interactions lasting more than 10 min in each experiment). (*E*) Reconstructed KikG$^+$KikR$^-$ cell volumes and KikR$^+$ cell volumes. (*F*) Interaction index (*SI Materials and Methods*). Each pair of red and green symbols represents one mouse.

KikG$^+$KikR$^-$ DCs (Fig. 5*E* and *SI Materials and Methods*). The resultant "interaction indexes" suggested that individual KikR$^+$ DCs are more capable of stably interacting with OT-I T cells than individual KikG$^+$KikR$^-$ DCs (Fig. 5*F*). A similar trend was observed when we performed imaging analysis using the 9-d illumination protocol to compare KikR$^+$ entire migratory DCs and KikG$^+$KikR$^-$ resident DCs (Fig. S5). Taken together, these results suggest that migratory DCs arriving in the SDLN after s.c. immunization with soluble antigen plus double-stranded RNA analog are most efficiently engaged in stable interactions with antigen-specific CD8$^+$ T cells.

Discussion

It is often argued that the immune system is organized to optimize the cell–antigen and cell–cell interactions underlying immune function. Indeed, the distinct properties and roles of DC subsets in T-cell activation and regulation may explain the physiological significance of the differential localization of DC subsets in the spleen and SDLNs (12, 23). Our studies on the DC localization in *Xcr1* reporter mice confirm the localization patterns suggested by computational processing of multicolor histological images: LN-resident CD8α^{hi} DCs and migratory CD103^{hi} DCs are enriched in the deep part of the T-cell zone in the SDLNs; CD11b$^+$ DCs are enriched near the lymphatic sinuses and conduits (12, 19). Our results suggest that this DC regionalization creates segregated locations for activation of antigen-specific CD4$^+$ T cells and CD8$^+$ T cells. Given recent findings (19), this may suggest that it is advantageous for CD11b$^+$ DCs to sample antigens from the LN sinuses and conduits for rapid CD4$^+$ T-cell activation; in contrast, antigen delivery for CD8$^+$ T-cell activation may be more dependent on migratory DCs that capture antigen in the skin and migrate to the T-cell zone of the SDLNs. This notion is consistent with our data showing that OT-II T-cell activation was somewhat faster than OT-I T-cell activation. Our results also suggest that migration of naive CD8$^+$ T cells and CD4$^+$ T cells in the T-cell zone is biased to facilitate scanning for their cognate DCs. This notion is also supported by the previous observation that naive CD4$^+$ T cells spend less time scanning the T-cell zone than naive CD8$^+$ T cells after their LN entry through HEVs near the conduits and before their exit from the sinuses (24).

During the revision of this paper, the spatiotemporal characterization of antigen-specific CD4$^+$ T cells and CD8$^+$ T cells in the SDLNs was reported in HSV-1 or vaccinia virus infection (25, 26). Although the location and/or timing of initial activation of CD4$^+$ T cells and CD8$^+$ T cells and the roles of XCR1$^+$ DCs vary, depending on the types of vaccines and microbes, these studies, together with ours, clearly indicate spatially or temporally segregated interactions of DC subsets with antigen-specific CD4$^+$ T cells and CD8$^+$ T cells.

Our data show that after immunization with soluble antigen and double-stranded RNA, *Xcr1*-expressing migratory DCs that have newly arrived in the SDLN interacted with antigen-specific CD8$^+$ T cells more prominently than other *Xcr1*-expressing DCs, i.e., LN-resident DCs and the migratory DCs that had arrived in the LNs before immunization. Future studies need to test whether the superior interaction ability is dependent on the prominent up-regulation of CD86 and CD80 by the newly arriving migratory DCs, because the costimulatory molecules can strengthen antigen-dependent interactions between T cells and DCs (27). It is also likely, but not certain, that the newly arriving migratory DCs present the highest amounts of peptides after they have encountered antigen plus double-stranded RNA in the skin. Nonetheless, we observed that a nonnegligible number of LN-resident DCs were stably interacting with antigen-specific CD8$^+$ T cells. LN-resident DCs can present antigen that has been transported either through lymphatic sinuses and conduits or through antigen transfer from the newly arriving migratory DCs (19, 28). In this sense, it is of note that a small fraction of *Xcr1*-expressing DCs near the LN capsule are predominantly LN-resident DCs. It will be needed to investigate whether *Xcr1*-expressing LN-resident DCs sample antigen from the subcapsular sinus and migrate to the T-cell zone for interacting with CD8$^+$ T cells. More importantly, future studies should perform similar imaging analyses with the *Xcr1*$^{KikGR/+}$ mouse strain during different types of immune responses, because capabilities of the migratory and resident DC subsets to interact with CD8$^+$ T cells are likely to be affected by the types of vaccines and microbes (17, 25, 26, 28).

In this study we have directly shown the immigration kinetics of *Xcr1*-expressing migratory DCs from the skin to the SDLNs. The turnover rate of these migratory DCs in the SDLNs from our photoconversion experiments is similar to the one reported previously: 9 d for the BrdU-labeled CD8$^+$DEC-205$^+$ DCs in the SDLNs, which were presumably a mixture of LN-resident CD8α^{hi} DCs and migratory CD103^{hi} DCs (29). A recent study used transgenic mice expressing KikGR ubiquitously to infer a shorter lifetime of MHC-II^{hi}CD103$^+$ DCs (4–5 d), likely to be the same population as migratory CD103^{hi} DCs in this study (30). The reason for this faster turnover is unclear, but it may reflect their more invasive method to surgically expose the SDLNs (30).

Turnover dynamics of LN-resident DCs could not be assessed in this study. However, a previous work reported that transferred DC precursors, which could give rise to LN-resident DCs including CD8α^{hi} DCs, primarily entered the SDLNs through HEVs in the medullary side and then appeared near the LN sinus in 6 d (31). This may suggest that LN-resident DCs in the deepest region of the T-cell zone are newly formed from DC precursors.

Because we have observed that the migratory DCs eventually reach the same region, it would be interesting to test in future studies whether antigen transfer occurs from the migratory DCs to the newly differentiated LN-resident DCs in this region (32).

Our previous work analyzing *Xcr1*-expressing DCs in various tissues using $Xcr1^{Venus/+}$ mice has shown that $CD103^{hi}$ DCs in the gut lamina propria and mesenteric LNs are expressing a similar level of Venus to that in $CD103^{hi}$ DCs in the SDLNs (16). The $CD103^{+}$ DCs in the lamina propria are thought to induce differentiation of naive $CD4^{+}$ T cells into regulatory T cells in the mesenteric LNs to establish immune tolerance in the gut (33, 34). However, much remains to be learned about migration dynamics of the $CD103^{hi}$ DCs from the lamina propria to the mesenteric LNs. The $Xcr1^{KikGR/+}$ mouse strain developed here will enable future studies to track the mucosal $CD103^{hi}$ DCs, providing insights into the mechanisms underlying T-cell regulation as well as T-cell activation.

Materials and Methods

Mice. All animal experiments were approved by the Animal Research Committees of RIKEN Yokohama Research Institute and Osaka University. Generation of the $Xcr1^{KikGR}$ mouse strain and information about the other mice are in *SI Materials and Methods*.

Photoconversion. Illumination of the mouse skin was performed as described in ref. 35 with some modifications. The details are described in *SI Materials and Methods*.

Intravital Two-Photon Microscopy. The inguinal LN of an anesthetized mouse was imaged by the TCS SP5 inverted microscope (Leica Microsystems) equipped with a Chameleon Ultra II Ti:Sapphire laser (Coherent). The details are described in *SI Materials and Methods*.

Image Analysis of Two-Photon Microscopy. Cell-tracking and cell–cell interaction analyses were performed using Imaris software (Bitplane) as described previously (36). The cell volume was obtained by using the "Cells" function of Imaris. The details are described in *SI Materials and Methods*.

Preparation of Vibratome Slices. Inguinal LNs embedded in an agarose gel were sagittally sliced by a VT1200 S vibrating blade microtome (Leica Microsystems). The slices were stained with antibodies and imaged by an SP5 II confocal microscope (Leica Microsystems). The details are described in *SI Materials and Methods*.

The other methods used in this study including flow cytometry, cell preparation, immunization, cryosection staining, and statistical analysis are described in detail in *SI Materials and Methods*.

ACKNOWLEDGMENTS. We thank I. Ogahara, Y. Fukuda, S. Moriyama, C. Tran, S. Takahashi, S. Fujii, and C. Allen for technical assistance and advice; J. Miyazaki for CAG-Cre mice; and T. Yano and M. Sugiyama for discussion and maintaining the mutant mice. This work was supported by a RIKEN Special Postdoctoral Researcher Program (M.K.); a Japan Society for The Promotion of Science Postdoctoral Fellowship for Research Abroad (to M.K.); a Human Frontier Science Program Long-Term Fellowship (to M.K.); the Translational Imaging Center, University of Southern California (M.K. and S.E.F.); and the Ministry of Education, Culture, Sports, Science, and Technology of Japan (M.K., T.K., and T.O.).

1. Mellman I, Steinman RM (2001) Dendritic cells: Specialized and regulated antigen processing machines. *Cell* 106(3):255–258.
2. Germain RN, Robey EA, Cahalan MD (2012) A decade of imaging cellular motility and interaction dynamics in the immune system. *Science* 336(6089):1676–1681.
3. Henrickson SE, et al. (2008) In vivo imaging of T cell priming. *Sci Signal* 1(12):pt2.
4. Moreau HD, Bousso P (2014) Visualizing how T cells collect activation signals in vivo. *Curr Opin Immunol* 26:56–62.
5. Joffre OP, Segura E, Savina A, Amigorena S (2012) Cross-presentation by dendritic cells. *Nat Rev Immunol* 12(8):557–569.
6. Lindquist RL, et al. (2004) Visualizing dendritic cell networks in vivo. *Nat Immunol* 5(12):1243–1250.
7. Liu K, Nussenzweig MC (2010) Origin and development of dendritic cells. *Immunol Rev* 234(1):45–54.
8. Bar-On L, Jung S (2010) Defining dendritic cells by conditional and constitutive cell ablation. *Immunol Rev* 234(1):76–89.
9. Heath WR, Carbone FR (2009) Dendritic cell subsets in primary and secondary T cell responses at body surfaces. *Nat Immunol* 10(12):1237–1244.
10. del Rio ML, Bernhardt G, Rodriguez-Barbosa JI, Förster R (2010) Development and functional specialization of CD103+ dendritic cells. *Immunol Rev* 234(1):268–281.
11. Kissenpfennig A, et al. (2005) Dynamics and function of Langerhans cells in vivo: Dermal dendritic cells colonize lymph node areas distinct from slower migrating Langerhans cells. *Immunity* 22(5):643–654.
12. Gerner MY, Kastenmuller W, Ifrim I, Kabat J, Germain RN (2012) Histo-cytometry: A method for highly multiplex quantitative tissue imaging analysis applied to dendritic cell subset microanatomy in lymph nodes. *Immunity* 37(2):364–376.
13. Bachem A, et al. (2012) Expression of XCR1 characterizes the Batf3-dependent lineage of dendritic cells capable of antigen cross-presentation. *Front Immunol* 3:214.
14. Yamazaki C, et al. (2010) Conservation of a chemokine system, XCR1 and its ligand, XCL1, between human and mice. *Biochem Biophys Res Commun* 397(4):756–761.
15. Dorner BG, et al. (2009) Selective expression of the chemokine receptor XCR1 on cross-presenting dendritic cells determines cooperation with CD8+ T cells. *Immunity* 31(5):823–833.
16. Yamazaki C, et al. (2013) Critical roles of a dendritic cell subset expressing a chemokine receptor, XCR1. *J Immunol* 190(12):6071–6082.
17. Bedoui S, et al. (2009) Cross-presentation of viral and self antigens by skin-derived CD103+ dendritic cells. *Nat Immunol* 10(5):488–495.
18. Sixt M, et al. (2005) The conduit system transports soluble antigens from the afferent lymph to resident dendritic cells in the T cell area of the lymph node. *Immunity* 22(1):19–29.
19. Gerner MY, Torabi-Parizi P, Germain RN (2015) Strategically localized dendritic cells promote rapid T cell responses to lymph-borne particulate antigens. *Immunity* 42(1):172–185.
20. Hogquist KA, et al. (1994) T cell receptor antagonist peptides induce positive selection. *Cell* 76(1):17–27.
21. Barnden MJ, Allison J, Heath WR, Carbone FR (1998) Defective TCR expression in transgenic mice constructed using cDNA-based alpha- and beta-chain genes under the control of heterologous regulatory elements. *Immunol Cell Biol* 76(1):34–40.
22. Tsutsui H, Karasawa S, Shimizu H, Nukina N, Miyawaki A (2005) Semi-rational engineering of a coral fluorescent protein into an efficient highlighter. *EMBO Rep* 6(3):233–238.
23. Dudziak D, et al. (2007) Differential antigen processing by dendritic cell subsets in vivo. *Science* 315(5808):107–111.
24. Mandl JN, et al. (2012) Quantification of lymph node transit times reveals differences in antigen surveillance strategies of naive CD4+ and CD8+ T cells. *Proc Natl Acad Sci USA* 109(44):18036–18041.
25. Eickhoff S, et al. (2015) Robust anti-viral immunity requires multiple distinct T cell-dendritic cell interactions. *Cell* 162(6):1322–1337.
26. Hor JL, et al. (2015) Spatiotemporally distinct interactions with dendritic cell subsets facilitates CD4+ and CD8+ T cell activation to localized viral infection. *Immunity* 43(3):554–565.
27. Lim TS, et al. (2012) CD80 and CD86 differentially regulate mechanical interactions of T-cells with antigen-presenting dendritic cells and B-cells. *PLoS One* 7(9):e45185.
28. Allan RS, et al. (2006) Migratory dendritic cells transfer antigen to a lymph node-resident dendritic cell population for efficient CTL priming. *Immunity* 25(1):153–162.
29. Kamath AT, Henri S, Battye F, Tough DF, Shortman K (2002) Developmental kinetics and lifespan of dendritic cells in mouse lymphoid organs. *Blood* 100(5):1734–1741.
30. Tomura M, et al. (2014) Tracking and quantification of dendritic cell migration and antigen trafficking between the skin and lymph nodes. *Sci Rep* 4:6030.
31. Liu K, et al. (2009) In vivo analysis of dendritic cell development and homeostasis. *Science* 324(5925):392–397.
32. Inaba K, et al. (1998) Efficient presentation of phagocytosed cellular fragments on the major histocompatibility complex class II products of dendritic cells. *J Exp Med* 188(11):2163–2173.
33. Sun CM, et al. (2007) Small intestine lamina propria dendritic cells promote de novo generation of Foxp3 T reg cells via retinoic acid. *J Exp Med* 204(8):1775–1785.
34. Coombes JL, et al. (2007) A functionally specialized population of mucosal CD103+ DCs induces Foxp3+ regulatory T cells via a TGF-beta and retinoic acid-dependent mechanism. *J Exp Med* 204(8):1757–1764.
35. Tomura M, et al. (2010) Activated regulatory T cells are the major T cell type emigrating from the skin during a cutaneous immune response in mice. *J Clin Invest* 120(3):883–893.
36. Kitano M, Okada T (2012) Four-dimensional tracking of lymphocyte migration and interactions in lymph nodes by two-photon microscopy. *Methods Enzymol* 506:437–454.
37. Sakai K, Miyazaki Ji (1997) A transgenic mouse line that retains Cre recombinase activity in mature oocytes irrespective of the cre transgene transmission. *Biochem Biophys Res Commun* 237(2):318–324.
38. Kitano M, et al. (2011) Bcl6 protein expression shapes pre-germinal center B cell dynamics and follicular helper T cell heterogeneity. *Immunity* 34(6):961–972.
39. Moriyama S, et al. (2014) Sphingosine-1-phosphate receptor 2 is critical for follicular helper T cell retention in germinal centers. *J Exp Med* 211(7):1297–1305.